

Morpheus Reveals Distant Disk Galaxy Morphologies with *JWST*: The First AI/ML Analysis of *JWST* Images

BRANT E. ROBERTSON ¹ SANDRO TACCHHELLA ^{2,3} BENJAMIN D. JOHNSON ⁴ RYAN HAUSEN ⁵
ADEBUSOLA B. ALABI ¹ KRISTAN BOYETT ^{6,7} ANDREW J. BUNKER ⁸ STEFANO CARNIANI ⁹ EIICHI EGAMI ¹⁰
DANIEL J. EISENSTEIN ⁴ KEVIN N. HAINLINE ¹⁰ JAKOB M. HELTON ¹⁰ ZHIYUAN JI ¹¹ NIMISHA KUMARI ¹²
JIANWEI LYU ¹⁰ ROBERTO MAIOLINO ^{2,3} ERICA J. NELSON ¹³ MARCIA J. RIEKE ¹⁰ IRENE SHIVAEI ¹⁰
FENGWU SUN ¹⁰ HANNAH ÜBLER ^{2,3} CHRISTINA C. WILLIAMS ^{14,10} CHRISTOPHER N. A. WILLMER ¹⁵ AND
JORIS WITSTOK ^{2,3}

¹Department of Astronomy and Astrophysics, University of California, Santa Cruz, 1156 High Street, Santa Cruz, CA 95064, USA

²Kavli Institute for Cosmology, University of Cambridge, Madingley Road, Cambridge, CB3 0HA, UK

³Cavendish Laboratory, University of Cambridge, 19 JJ Thomson Avenue, Cambridge, CB3 0HE, UK

⁴Center for Astrophysics | Harvard & Smithsonian, 60 Garden Street, Cambridge, MA 02138, USA

⁵Department of Physics and Astronomy, The Johns Hopkins University, 3400 N. Charles St., Baltimore, MD 21218, USA

⁶School of Physics, University of Melbourne, Parkville 3010, VIC, Australia

⁷ARC Centre of Excellence for All Sky Astrophysics in 3 Dimensions (ASTRO 3D), Australia

⁸Department of Physics, University of Oxford, Denys Wilkinson Building, Keble Road, Oxford OX13RH, U.K.

⁹Scuola Normale Superiore, Piazza dei Cavalieri 7, I-56126 Pisa, Italy

¹⁰Steward Observatory, University of Arizona, 933 N. Cherry Avenue, Tucson, AZ 85721, USA

¹¹University of Massachusetts Amherst, 710 North Pleasant Street, Amherst, MA 01003-9305, USA

¹²AURA for the European Space Agency, Space Telescope Science Institute, 3700 San Martin Drive, Baltimore, MD 21218, USA

¹³Department for Astrophysical and Planetary Science, University of Colorado, Boulder, CO 80309, USA

¹⁴NSF's National Optical-Infrared Astronomy Research Laboratory, 950 N. Cherry Avenue, Tucson, AZ 85719, USA

¹⁵Steward Observatory, University of Arizona, 933 North Cherry Avenue, Tucson, AZ 85721, USA

ABSTRACT

The dramatic first images with *James Webb Space Telescope* (*JWST*) demonstrated its power to provide unprecedented spatial detail for galaxies in the high-redshift universe. Here, we leverage the resolution and depth of the *JWST* Cosmic Evolution Early Release Science Survey (CEERS) data in the Extended Groth Strip (EGS) to perform pixel-level morphological classifications of galaxies in *JWST* *F150W* imaging using the *Morpheus* deep learning framework for astronomical image analysis. By cross-referencing with existing photometric redshift catalogs from the *Hubble Space Telescope* (*HST*) CANDELS survey, we show that *JWST* images indicate the emergence of *disk* morphologies before $z \sim 2$ and with candidates appearing as early as $z \sim 5$. By modeling the light profile of each object and accounting for the *JWST* point-spread function, we find the high-redshift disk candidates have exponential surface brightness profiles with an average Sérsic (1968) index $\langle n \rangle = 1.04$ and $> 90\%$ displaying “disky” profiles ($n < 2$). Comparing with prior *Morpheus* classifications in CANDELS we find that a plurality of *JWST* disk galaxy candidates were previously classified as *compact* based on the shallower *HST* imagery, indicating that the improved optical quality and depth of the *JWST* helps to reveal disk morphologies that were hiding in the noise. We discuss the implications of these early disk candidates on theories for cosmological disk galaxy formation.

1. INTRODUCTION

The formation and evolution of disk galaxies in the context of our Λ CDM cosmology remains as one of the most complex problems in astrophysics. The violent, hierarchical nature of galaxy mass assembly at high redshifts can destroy dynamically cold disks, and yet thin disk galaxies are plentiful in the local universe. Determining the era when the first disk galaxies could form

would provide an important milestone in understanding how galaxy morphology develops over cosmic time. This *Letter* presents first results of applying artificial intelligence/machine learning (AI/ML) techniques to *James Webb Space Telescope* (*JWST*) images, searching for distant disk galaxies by analyzing *JWST* data with the *Morpheus* deep learning framework (Hausen & Robertson 2020, hereafter H20).

Observations of disk galaxy formation in the distant universe have advanced greatly over the last two decades. Integral field spectroscopy of disk galaxies at intermediate redshifts ($z \sim 2$) established that the ionized gas dynamics of many early-forming disks differed substantially from those in the local universe, with lower ratios of rotational velocity to velocity dispersion V/σ than in the present day (e.g., Genzel et al. 2006; Law et al. 2007; Genzel et al. 2008; Stott et al. 2016; Simons et al. 2017; Förster Schreiber et al. 2018; Wisnioski et al. 2019). Large, star-forming disk galaxies at redshifts $z \sim 1 - 3$ can be baryon-dominated, with relatively little dark matter contributing to their rotation curves (Wuyts et al. 2016; Genzel et al. 2017; Übler et al. 2018; Price et al. 2020; Genzel et al. 2020). The structure of early disks can be distinct from dynamically colder disk galaxies at the present, perhaps reflecting a transition between disks heavily influenced by the hierarchical mass assembly process to more ordered rotation at lower redshifts (e.g., Kassin et al. 2012; Simons et al. 2017; Tiley et al. 2021). This transition may mirror the evolution of observed axis ratios, as observations with *HST* have established a smaller fraction of disk galaxies at earlier cosmic times (e.g., Law et al. 2012; van der Wel et al. 2014; Zhang et al. 2019).

Observations of [CIII] and CO emission at even higher redshifts with the *Atacama Large Millimeter/Submillimeter Array* (*ALMA*) have discovered evidence for rotationally-supported disk galaxies in the first two billion years of cosmic history (Smit et al. 2018; Neeleman et al. 2020; Rizzo et al. 2020, 2021; Fraternali et al. 2021; Lelli et al. 2021; Tsukui & Iguchi 2021). These $z > 4$ galaxies show $V/\sigma \sim 10 - 20$, substantially larger than those predicted for the bulk population of disk galaxies by cosmological simulations (e.g., Pillepich et al. 2019). Recent theoretical work suggests that relatively massive galaxies may sustain cold disks even in the early universe (Kretschmer et al. 2022; Gurvich et al. 2022), but understanding how rare such objects are, elucidating the role of the kinematical tracer, and determining their relationship to the broader galaxy population all require more investigation.

The new *JWST* data can address outstanding questions raised by these previous results. When did the first disk galaxy candidates appear in the universe? What is the relative gas to stellar mass content of these galaxies, and how does that influence their formation? *JWST* can contribute substantially to answering these questions, both through better constraints on the stellar population properties of early disks and through kinematic measures via its unprecedented spectroscopic capabilities. Addressing these questions with *JWST* will require

the identification of more high-redshift disk galaxy candidates. Here, we perform pixel-level analysis of the *JWST* Cosmic Evolution Early Release Science Survey (CEERS; Finkelstein et al., in prep.) data in the Extended Groth Strip (EGS) using the *Morpheus* deep learning model (H20) to search for high-redshift ($z > 2$) disk galaxy candidates. *Morpheus* has been trained to classify galaxies, stars, and sky pixels in space-based astronomical images, and we apply the model directly to the EGS *JWST F150W* mosaic without modification. We identify galaxies with photometric redshifts $z > 2$ with dominant disk morphologies as determined by *Morpheus*. We then verify via surface brightness model fitting that the vast majority of candidates are structurally consistent with being high-redshift disks. These results indicate that AI/ML methods like *Morpheus* will effectively identify distant disk galaxy candidates for kinematic follow-up observations with spectroscopy. Our AI/ML approach complements other recent work identifying disk galaxy candidates in deep *JWST* images through traditional analyses (e.g., Fudamoto et al. 2022; Nelson et al. 2022; Ferreira et al. 2022; Jacobs et al. 2022; Wu et al. 2022). Where necessary, we assume parameters for the flat Λ CDM cosmology determined by the Planck Collaboration et al. (2020) survey (i.e., $h = 0.674$, $\Omega_m = 0.315$).

2. METHOD

The identification of high-redshift disk galaxy candidates in the *JWST* CEERS images proceeded by first fully re-reducing the imaging data products and then performing object detection and photometry (§2.1). We then analyzed the *JWST F150W* images with *Morpheus* to identify objects with disk morphologies (§2.2), and cross-referenced with catalogs from the literature to select disk candidates at $z > 2$ (§2.3).

2.1. Imaging, Detection, and Photometry

The *JWST* CEERS EGS images (34.5 arcmin², see Finkelstein et al. 2022, Finkelstein in prep.) were downloaded and processed with the STScI *JWST* pipeline (v1.6.2) using custom treatments for data artifacts to remove “wisps” and “snowballs” (e.g., §6 of Rigby et al. 2022), background subtraction and sky flats (`jwst_0953.pmap`), and $1/f$ -noise correction. The exposures were astrometrically aligned to the CEERS *HST F160W* image and mosaiced onto a 0.03”/pixel image.

Object detection and photometry were performed using a set of custom scripts based on *photutils* methods. We created a detection image from an inverse-variance weighted stack of the long-wavelength *F277W*, *F356W*, *F410M*, and *F444W* mosaics to provide a deep, rest-

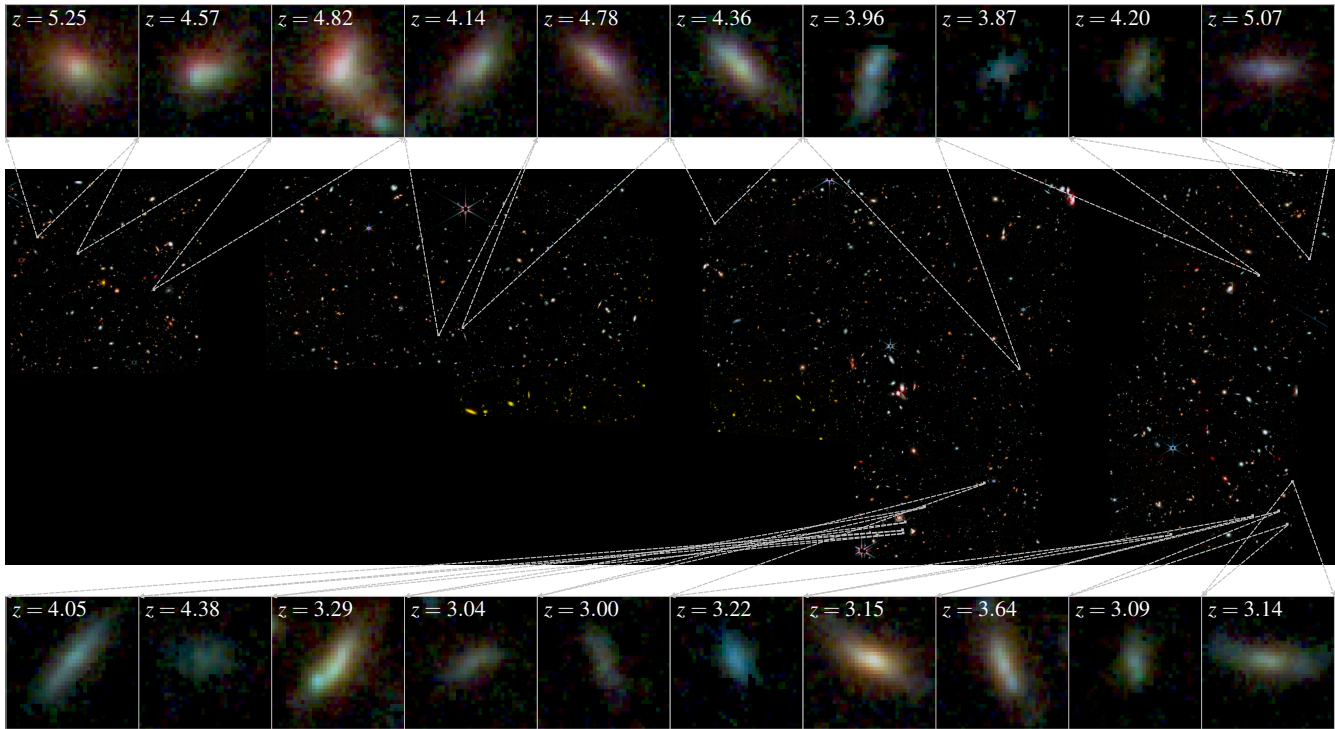


Figure 1. High-redshift disk galaxy candidates selected by the *Morpheus* AI/ML classifier in the CEERS EGS *JWST* imagery. Shown is a *JWST* *F444W-F200W-F115W* RGB false-color image (center) along with thumbnails of the 20 highest redshift disk galaxy candidates (top and bottom rows). Most disk galaxy candidates selected by *Morpheus* show flattened, extended light distributions consistent with disk morphologies.

frame optical selection. Contiguous regions in the detection image with pixels $SNR > 5$ were identified as objects in a segmentation map, and forced aperture photometry was performed about their centroids.

2.2. Morphological Analysis

The *JWST* *F150W* images were analyzed using a version of *Morpheus* (H20) trained on *HST* *F160W* images at a similar observed wavelength. *Morpheus* is a UNet (Ronneberger et al. 2015) convolutional neural network with residual links (He et al. 2015) that performs pixel-level classification, assigning a “model probability” that each pixel in a science-quality FITS image (Wells et al. 1981) belongs to *spheroid*, *disk*, *irregular*, *compact/point source*, or *background* classes. A “classification image” for each class is produced to record the pixel-level model probabilities, which can be agglomerated into object-level classifications by summations over the pixels. H20 used the visual classifications of CANDELS galaxies provided by Kartaltepe et al. (2015) (90% completeness limit for an $H < 24.5AB$ selection) to train the model, and then used *Morpheus* to classify all the pixels in CANDELS by processing the *HST* *F606W*, *F814W*, *F125W*, and *F160W* images. *Morpheus* has since been updated to include an accelerated attention mechanism (Wang et al. 2017; Vaswani

et al. 2017; Hu et al. 2020) that improves the model performance by using non-local image features and allows for larger regions of the image to be classified at once, providing a roughly $100\times$ speed up in classification efficiency relative to H20 with comparable performance (for a discussion of related changes to *Morpheus*, see Hausen & Robertson 2022). The updated *Morpheus* model was previously trained to perform classification on *HST* *F160W* images alone using the Adam optimizer (Kingma & Ba 2014). We leverage this training to provide a first attempt at classification of the *JWST* *F150W* images at a similar observed wavelength and validate our classifications with surface brightness profile modeling.

2.3. Disk Galaxy Candidate Selection

To identify disk galaxy candidates, we used the *Morpheus* classification images with the segmentation maps and detection images (see §2.1) to create SNR-weighted object-level model probabilities for each class. We cross-matched our sources against the CANDELS v1 EGS photometric redshift and stellar population synthesis analysis catalogs (Stefanon et al. 2017), and then selected all objects at redshifts $z \geq 2$ with a *Morpheus*-assigned object-level model probability $p(\text{disk}) > 0.5$. For this initial analysis, we restrict our sample to ob-

jects with photometric redshift estimates available in the CANDELS catalogs (90% complete for point sources $F160W < 26.62$, see [Stefanon et al. 2017](#), for details on detection and photometric redshift determinations) and spatially close centroid matches ($\lesssim 5$ pixels). Over the NIRC*am* EGS footprint, we find good spatial matches to ~ 7700 sources in the CANDELS catalog before redshift or morphological cuts. Over all redshifts, about 1600 CANDELS EGS sources are classified as *disk* by *Morpheus*.

3. RESULTS

The selection criteria (§2.3) applied to the analysis of *JWST* NIRC*am* images with *Morpheus* (§2.2) identified 202 disk galaxy candidates out of 2507 catalog matches with redshifts $z \geq 2$. The average photometric redshift of the sample is $\langle z \rangle = 2.67$, with 42 disk candidates at redshifts $z > 3$ (out of 988) and 10 disk candidates at redshifts $z > 4$ (out of 353). Below, we examine the visual morphologies of the objects (§3.1) and perform surface brightness model fitting to verify consistency with structural disk galaxy properties (§3.2).

3.1. Visual Morphologies

Figure 1 shows a *JWST* $F444W$ - $F200W$ - $F115W$ RGB false color image of the CEERS EGS mosaic, highlighting 20 candidates with large CANDELS photometric redshifts as $0.3'' \times 0.3''$ thumbnails above and below the mosaic. Many candidates show disk-like visual morphologies, often with flattened, extended light distributions. Some galaxies show central concentrations, clumps, or amorphous light distributions in addition to their extended disk morphologies. Of the 202 high-redshift disk candidates, only 21% were brighter than the $H < 24.5$ AB completeness limit for visual classification by [Kartaltepe et al. \(2015\)](#) and of these 57% were classified as *disk* in our prior *HST*-based analysis. Of the 160 objects fainter than $H = 24.5$ AB, only 8 (5%) were previously classified as *disk*. The plurality (49%) of objects were previously classified as *compact/point source* as the *HST* imaging quality was not detailed or deep enough for the model to choose a distinctive morphology for many objects. The remaining objects were previously classified as *spheroid* (5%), *irregular* (16%), or not detected by the algorithm and labeled as *background* (25%). To compare with previous AI/ML classifications, over 800 arcmin^2 of *HST* CANDELS images [Huertas-Company et al. \(2016\)](#) reported finding 413 objects with redshifts $z > 2$ that they classify as disks, whereas with *Morpheus* applied to *JWST* $F150W$ we find 202 candidate *disk* galaxies at $z > 2$ over only 34.5 arcmin^2 . Given the wide range of redshifts $z \sim 2 - 5$, the colors of the objects vary with

$F115W - F150W \approx 0 - 1$ AB and $F150W - F200W \approx -0.1 - 0.6$ AB, and mean colors $\langle F115W - F150W \rangle = 0.51$ AB and $\langle F150W - F200W \rangle = 0.17$ AB. From the CANDELS catalogs, we find that the typical stellar masses are $\langle \log M_*/M_\odot \rangle = 9.13 \pm 0.48$, with 40% of objects inferred to have less than a billion solar masses in stars.

3.2. Surface Brightness Profiles

Following the identification of high-redshift disk galaxy candidates by *Morpheus*, an evaluation of the candidates through a traditional morphological analysis can help assess the efficacy of our AI/ML approach even without retraining on *JWST* images. If traditional metrics of “diskiness” agree with the *Morpheus* results, our confidence in the AI/ML classifications would be strengthened. In [Hausen & Robertson \(2020\)](#), the ability of *Morpheus* to classify Sérsic (1968) profiles based on traditional associations between surface brightness profile and morphology was demonstrated. *Morpheus* classifies extended objects with $n = 1$ Sérsic indices (exponential profiles) as *disk*, whereas objects with $n \geq 4$ indices are usually classified as *spheroid* or *compact/point source*. In this work, we used the *forcepho* ([Johnson et al., in prep.](#)) and *ProFit* ([Robotham et al. 2017](#)) Bayesian profile fitting codes to model the surface brightness profile of each high-redshift disk galaxy candidate selected by *Morpheus*. We note that *Morpheus* can spatially distinguish between the bulge and disk components of galaxies, and can also classify pixels in the star-forming regions of disks as *irregular* (see H20). We will explore these composite morphologies in *JWST* imagery in future work.

3.2.1. ForcePho Modeling

When using *forcepho*, a $3'' \times 3''$ region about each object centroid was cutout from the *JWST* $F115$, $F150W$, and $F200W$ flux and flux error images. Source locations from the detection catalog were supplied to *forcepho*, which then fit Sérsic models to the surface brightness profiles of each object in the cutout, accounting for possible flux contributions from neighboring sources. The PSFs used in convolving the models to the data resolution were generated from a mixture of Gaussians matched to reproduce the pre-flight *WebbPSF* ([Perrin et al. 2014](#)) model for each *JWST* filter. The *forcepho* code performs Monte Carlo Markov Chain sampling of the nine free parameters including $F115W$, $F150W$, $F200W$ fluxes, the RA and DEC of each object, the isophotal position angle, the axis ratio, the Sérsic index, and the half-light radius. This procedure allows for uncertainties on the model parameters to be computed and possible parameter covariances to be studied. A single

profile shape is fit to each filter by allowing only the amplitude to vary between them, and we do not attempt here to model wavelength-dependent shape variations.

3.2.2. ProFit Modeling

For the *ProFit* modeling, a $3'' \times 3''$ region about each object centroid was cutout from the *JWST F150W* flux and flux error images. These images, along with corresponding cutouts from the segmentation map and a PSF model generated by *WebbPSF*, were supplied to *ProFit* and a single-component Sérsic model was fit to each image. We used eight free parameters, including the pixel centroids, total flux, effective radius, Sérsic profile indices ($0.5 < n < 20$), axis ratio, position angle, and isophotal boxiness. One hundred and ninety out of 202 objects received successful *ProFit* fits, with the reduced $\langle \chi^2_\nu \rangle = 0.92 \pm 0.30$ for the sample. Failed *ProFit* single component fits showed evidence for multiple components, and many of these objects were successfully modeled with *forcepho*.

3.2.3. Surface Brightness Profile Model Results

Figure 2 shows a histogram of the best-fit Sérsic indices for the entire *Morpheus* high-redshift disk sample from *ProFit* modeling. The vast majority (183/190; 96%) of the successful fits displayed “disky” ($n < 2$) Sérsic indices, with a mean of $\langle n \rangle = 1.04$ and median $\hat{n} = 0.93$. The *forcepho* model fits show good agreement, with mean and median Sérsic indices of $\langle n \rangle = 1.06$ and $\hat{n} = 0.85$, and 97% of the disk candidates displaying $n < 2$. Figure 3 presents three example high-redshift disk galaxy candidates identified by *Morpheus* with photometric redshifts of $z \sim 2.3 - 5.2$. Shown are the *Morpheus* pixel-level classification maps for each object (left panels), their *JWST F150W* flux images (center left panels), the best-fit *forcepho* models of their surface brightness distributions (center right panels), and the residuals between the model and the data (right panels). As these examples demonstrate, the objects *Morpheus* classified as disks appear flattened and have best-fit Sérsic profiles with indices $n \sim 1$ as expected for exponential disks. In summary, the AI/ML classifications from *Morpheus* and the traditional Sérsic index morphological correspondence show excellent agreement. See H20 for more details on how *Morpheus* classifies galaxies with Sérsic profiles.

Beyond Sérsic index, the distribution of axis ratios can be used to assess the fraction of our candidates that are likely to be disks rather than prolate, potentially triaxial spheroids. Both the *forcepho* and *ProFit* models show very consistent axis ratios, with typical $\langle b/a \rangle \approx 0.4$ with a spread $0.2 < b/a < 1$. We follow Law et al. (2012) and perform Monte Carlo simulations of disks

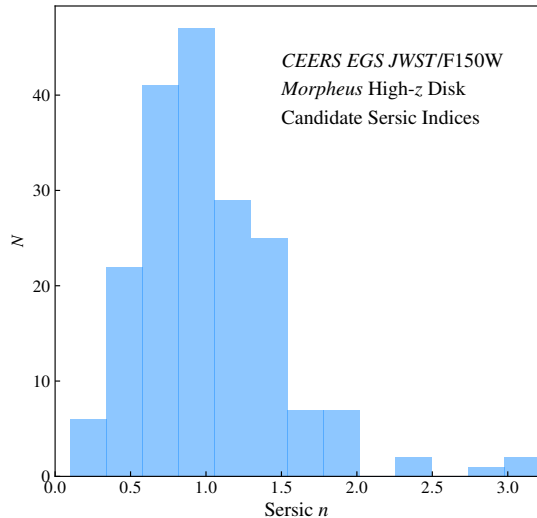


Figure 2. High-redshift disk candidate surface brightness profile (Sérsic 1968) indices determined by *ProFit* (Robotham et al. 2017). Shown is a histogram of the best-fit Sérsic index determined by fits to a $3'' \times 3''$ cutout of the *JWST F150W* flux and error images about each candidate selected by *Morpheus*. The mean Sérsic index of the sample is $\langle n \rangle = 1.04$, characteristic of exponential profiles traditionally associated with disk galaxies. A single source with a Sérsic index $n = 4.9$ was omitted from the histogram for clarity. Profile fits with *forcepho* (Johnson et al., in prep.) provide independent confirmation of the distribution, with 97% of high-redshift disk candidates displaying $n < 2$.

and spheroid projected axis ratio distributions. We then use a Kolmogorov-Smirnov test to compare consistency between the model and observed axis ratio distribution. Since the distributions are not uniform, and given prior *HST* results (e.g., Law et al. 2012; van der Wel et al. 2014; Zhang et al. 2019), we expect spheroids to contribute to the population of flattened, low-Sérsic objects and so not all of our candidates will truly be disks. Given the measured axis ratio distributions, we find an upper limit (3σ) that 57% of the sample can be pure disks with $b/a < 0.25$ with the remainder being triaxial or prolate spheroids. We cannot yet rule out a mix of triaxial spheroids with a wide range of axis ratios contributing to the majority of the sample. We also note that there is evidence from H20 that *Morpheus* is incomplete for face-on disks, and we expect this issue to be exacerbated for faint objects. Correcting for this incompleteness would raise the upper limits on pure disks. We leave a more detailed analysis for future work, but suggest that kinematic measurements from spectroscopic observations will be required to confirm our candidates as high-redshift disks.

4. DISCUSSION

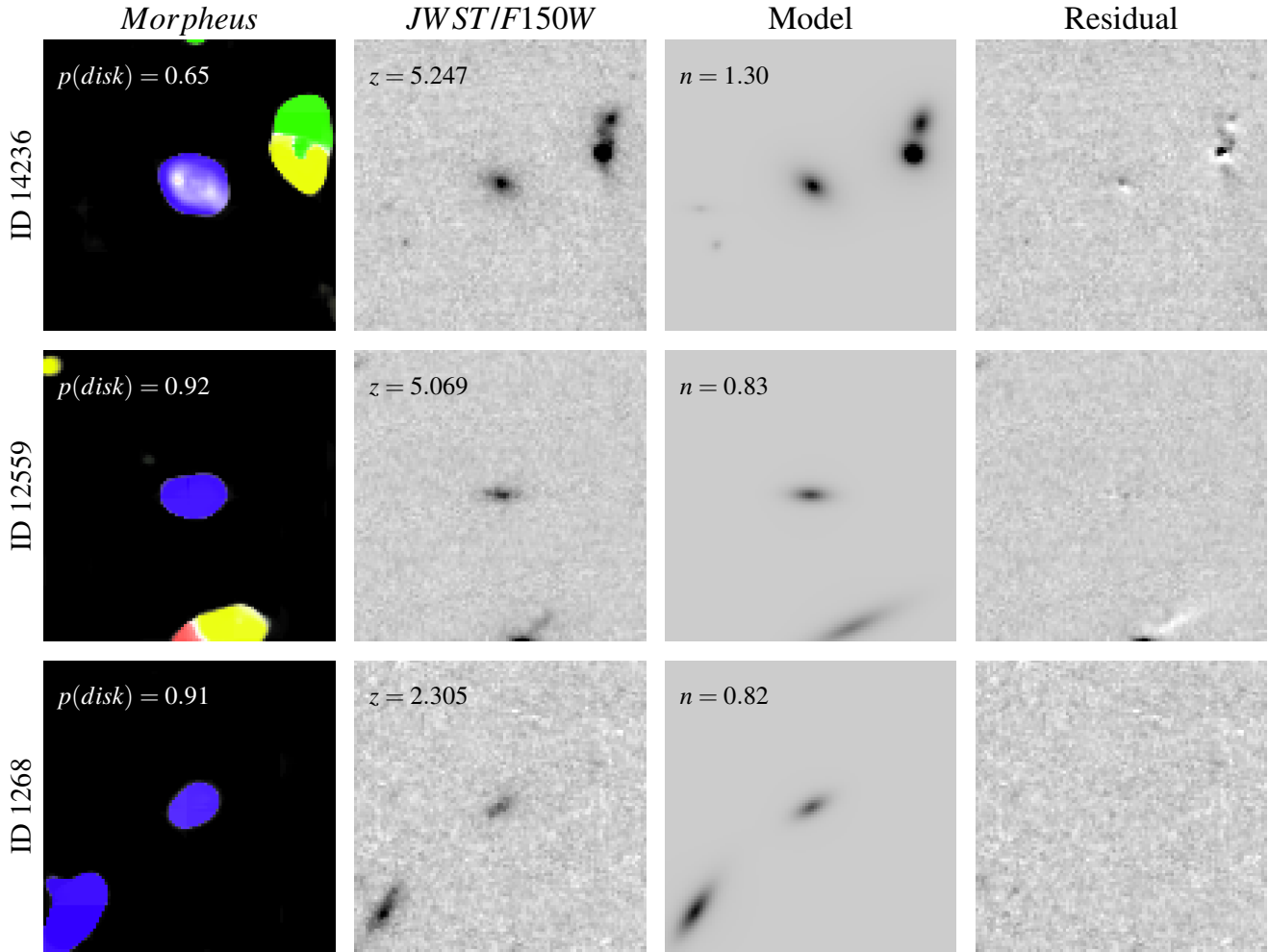


Figure 3. High-redshift disk galaxy candidate identification and modeling. The CEERS *JWST* *F150W* images were analyzed using the AI/ML model *Morpheus* to produce pixel-level classification images, and objects were selected as disk candidates based on SNR image-weighted averages of the pixel-level classifications. The left panels show the *Morpheus* pixel-level classification of three objects (*disk*:blue, *irregular*:green, *compact/point source*:yellow, *spheroid*:red, *indeterminant*:white), with $p(\text{disk}) \approx 0.65 - 0.92$. These objects were cross-referenced with the CANDELS photometric redshift catalog (Stefanon et al. 2017) to select objects at $z > 2$ (redshifts noted in center left panels). Surface brightness models of the *JWST* *F115W*, *F150W*, *F200W* object cutouts ($3'' \times 3''$; *F150W* shown center left) were modeled using the *forcepho* code (Johnson et al., in prep.), and Sérsic (1968) profile indices determined (center right panels). The small residuals between the *JWST* *F150W* images and models indicate high-quality fits (right panels). All grayscale images shown are displayed with the same linear stretch.

The ability of *JWST* to perform AI/ML-aided identification of distant disk galaxy candidates will add to the growing observational information we have on how early disk galaxies might form in our Λ CDM cosmology. Many of our disk candidates lie at $z \sim 2 - 3$ where there are substantial constraints on disk kinematical structure (e.g., Förster Schreiber & Wuyts 2020), but less is known about the high-redshift end of our sample. Recent *Atacama Large Millimeter/Submillimeter Array* (*ALMA*) observations, when combined with stellar population modeling, suggest that early star-forming main-sequence galaxies are extremely gas-rich ($\sim 90\%$; Heintz et al. 2022). *ALMA* observations of [CII] also show evidence

of rotating disk galaxies as early as $z \sim 5.5$ (Herrera-Camus et al. 2022) and rotation in quasars as early as $z \sim 6.5$ (Yue et al. 2021). As techniques for identifying high-redshift disk galaxies with *JWST* become more refined, including the first results from AI/ML techniques presented here, possible targets for gas kinematical measurements will become more prevalent. In principle, the *JWST* NIRSpect integral field unit spectrograph could also help reveal the kinematics of these disk candidates and confirm or refute the connection between the visual morphology and dynamical structure of these objects.

Early forming disk galaxies place important constraints on our theories of disk galaxy formation. While

cosmological simulations of disk galaxy formation found only moderate success (e.g., Robertson et al. 2004; Governato et al. 2007), more recent simulations have made substantial advances in reproducing disk galaxy morphologies (e.g., Aumer et al. 2013; Marinacci et al. 2014; Wetzel et al. 2016; Grand et al. 2017; El-Badry et al. 2018; Pillepich et al. 2019; Libeskind et al. 2020). However, disk formation at early epochs still remains challenging theoretically, especially for systems with large rotational support. The large V/σ seen in some early-forming systems (e.g., Neeleman et al. 2020; Rizzo et al. 2020, 2021; Fraternali et al. 2021; Lelli et al. 2021; Tsukui & Iguchi 2021) does not appear in the bulk population of $z \sim 2-5$ disks simulated cosmologically (e.g., Pillepich et al. 2019), although there are recent reports of success for individual simulated galaxies (Kretschmer et al. 2022; Gurvich et al. 2022; Segovia Otero et al. 2022) and very early populations of disks at $z > 8$ (Feng et al. 2015). The presence of these early disks may be sensitive to the galaxy mass (Gurvich et al. 2022) and the gas-rich merger history (e.g., Robertson et al. 2006). Identifying candidate early disk galaxies and characterizing their population properties will help us refine our picture for disk galaxy formation and understand the cosmological evolution of galaxy morphology. The combination of *JWST* and AI/ML techniques like *Morpheus* appears promising for identifying distant disk galaxy candidates for further study.

5. SUMMARY

We present first results applying AI/ML analysis to *JWST* imagery, using the *Morpheus* deep-learning framework for pixel-level astronomical image analysis with the *JWST* Cosmic Evolution Early Release Science Survey (CEERS; Finkelstein et al., in prep.) data in the Extended Groth Strip (EGS) to identify high-redshift ($z > 2$) disk galaxy candidates. We selected objects with dominant *disk* classifications determined by *Morpheus* ($p(\text{disk}) > 0.5$) and photometric redshifts $z > 2$ as determined by the CANDELS survey catalogs (Stefanon et al. 2017), identifying 202 high-redshift disk galaxy candidates. We then use the *ProFit* surface brightness distribution fitting code (Robotham et al.

2017) to infer single component (Sérsic 1968) profiles from the *JWST* *F150W* images. We find the high-redshift disk galaxy candidates identified by *Morpheus* predominantly display exponential (Sérsic $n = 1$) profiles common for disk galaxy morphologies, with an average Sérsic index of $\langle n \rangle = 1.04$. We conclude that *Morpheus* identifies galaxies as disks that would be so classified by traditional methods, and that *Morpheus* shows surprising efficacy at disk classification even as it was trained on *HST* *F160W* images and was applied to the *JWST* *F150W* mosaics without any modification. The identification of high-redshift disk galaxy candidates in *JWST* imagery suggests that disk galaxies may form early, with candidates in our sample displaying photometric redshifts as early as $z \sim 5$, and may indicate an early epoch of gas-rich disk formation through hierarchical processes in the early universe (e.g., Robertson et al. 2006). This work motivates further spectroscopic observations of high-redshift disk candidates to constrain their kinematical structure.

BER thanks Alice Shapley for a helpful discussion that in part motivated this work. BDJ, BER, CNAW, DJE, and MJR acknowledge support from the NIRCAM Science Team contract to the University of Arizona, NAS5-02015. The authors acknowledge use of the lux supercomputer at UC Santa Cruz, funded by NSF MRI grant AST 1828315. Funding for this research was provided by the Johns Hopkins University, Institute for Data Intensive Engineering and Science (IDIES). AJB acknowledges funding from the “FirstGalaxies” Advanced Grant from the European Research Council (ERC) under the European Union’s Horizon 2020 research and innovation programme (Grant agreement No. 789056). JW gratefully acknowledges support from the ERC Advanced Grant 695671, “QUENCH”, and the Fondation MERAC.

Software: astropy (Astropy Collaboration et al. 2013, 2018), *forcepho* (Johnson et al., in prep.), *Morpheus* (Hausen & Robertson 2020), *ProFit* (Robotham et al. 2017), TensorFlow (Abadi et al. 2016), WebbPSF (Perrin et al. 2014)

REFERENCES

- Abadi, M., Agarwal, A., Barham, P., et al. 2016, arXiv e-prints, arXiv:1603.04467.
<https://arxiv.org/abs/1603.04467>
- Astropy Collaboration, Robitaille, T. P., Tollerud, E. J., et al. 2013, *A&A*, 558, A33, doi: 10.1051/0004-6361/201322068
- Astropy Collaboration, Price-Whelan, A. M., Sipőcz, B. M., et al. 2018, *AJ*, 156, 123, doi: 10.3847/1538-3881/aabc4f
- Aumer, M., White, S. D. M., Naab, T., & Scannapieco, C. 2013, *MNRAS*, 434, 3142, doi: 10.1093/mnras/stt1230
- El-Badry, K., Quataert, E., Wetzel, A., et al. 2018, *MNRAS*, 473, 1930, doi: 10.1093/mnras/stx2482

- Feng, Y., Di Matteo, T., Croft, R., et al. 2015, *ApJL*, 808, L17, doi: [10.1088/2041-8205/808/1/L17](https://doi.org/10.1088/2041-8205/808/1/L17)
- Ferreira, L., Adams, N., Conselice, C. J., et al. 2022, arXiv e-prints, arXiv:2207.09428. <https://arxiv.org/abs/2207.09428>
- Finkelstein, S. L., Bagley, M. B., Arrabal Haro, P., et al. 2022, arXiv e-prints, arXiv:2207.12474. <https://arxiv.org/abs/2207.12474>
- Förster Schreiber, N. M., & Wuyts, S. 2020, *ARA&A*, 58, 661, doi: [10.1146/annurev-astro-032620-021910](https://doi.org/10.1146/annurev-astro-032620-021910)
- Förster Schreiber, N. M., Renzini, A., Mancini, C., et al. 2018, *ApJS*, 238, 21, doi: [10.3847/1538-4365/aadd49](https://doi.org/10.3847/1538-4365/aadd49)
- Fraternali, F., Karim, A., Magnelli, B., et al. 2021, *A&A*, 647, A194, doi: [10.1051/0004-6361/202039807](https://doi.org/10.1051/0004-6361/202039807)
- Fudamoto, Y., Inoue, A. K., & Sugahara, Y. 2022, arXiv e-prints, arXiv:2208.00132. <https://arxiv.org/abs/2208.00132>
- Genzel, R., Tacconi, L. J., Eisenhauer, F., et al. 2006, *Nature*, 442, 786, doi: [10.1038/nature05052](https://doi.org/10.1038/nature05052)
- Genzel, R., Burkert, A., Bouché, N., et al. 2008, *ApJ*, 687, 59, doi: [10.1086/591840](https://doi.org/10.1086/591840)
- Genzel, R., Förster Schreiber, N. M., Übler, H., et al. 2017, *Nature*, 543, 397, doi: [10.1038/nature21685](https://doi.org/10.1038/nature21685)
- Genzel, R., Price, S. H., Übler, H., et al. 2020, *ApJ*, 902, 98, doi: [10.3847/1538-4357/abb0ea](https://doi.org/10.3847/1538-4357/abb0ea)
- Governato, F., Willman, B., Mayer, L., et al. 2007, *MNRAS*, 374, 1479, doi: [10.1111/j.1365-2966.2006.11266.x](https://doi.org/10.1111/j.1365-2966.2006.11266.x)
- Grand, R. J. J., Gómez, F. A., Marinacci, F., et al. 2017, *MNRAS*, 467, 179, doi: [10.1093/mnras/stx071](https://doi.org/10.1093/mnras/stx071)
- Gurvich, A. B., Stern, J., Faucher-Giguère, C.-A., et al. 2022, arXiv e-prints, arXiv:2203.04321. <https://arxiv.org/abs/2203.04321>
- Hausen, R., & Robertson, B. 2022, arXiv e-prints, arXiv:2201.04714. <https://arxiv.org/abs/2201.04714>
- Hausen, R., & Robertson, B. E. 2020, *ApJS*, 248, 20, doi: [10.3847/1538-4365/ab8868](https://doi.org/10.3847/1538-4365/ab8868)
- He, K., Zhang, X., Ren, S., & Sun, J. 2015, arXiv e-prints, arXiv:1512.03385. <https://arxiv.org/abs/1512.03385>
- Heintz, K. E., Oesch, P. A., Aravena, M., et al. 2022, arXiv e-prints, arXiv:2206.07763. <https://arxiv.org/abs/2206.07763>
- Herrera-Camus, R., Förster Schreiber, N. M., Price, S. H., et al. 2022, arXiv e-prints, arXiv:2203.00689. <https://arxiv.org/abs/2203.00689>
- Hu, P., Perazzi, F., Caba Heilbron, F., et al. 2020, arXiv e-prints, arXiv:2007.03815. <https://arxiv.org/abs/2007.03815>
- Huertas-Company, M., Bernardi, M., Pérez-González, P. G., et al. 2016, *MNRAS*, 462, 4495, doi: [10.1093/mnras/stw1866](https://doi.org/10.1093/mnras/stw1866)
- Jacobs, C., Glazebrook, K., Calabrò, A., et al. 2022, arXiv e-prints, arXiv:2208.06516. <https://arxiv.org/abs/2208.06516>
- Kartaltepe, J. S., Mozena, M., Kocevski, D., et al. 2015, *ApJS*, 221, 11, doi: [10.1088/0067-0049/221/1/11](https://doi.org/10.1088/0067-0049/221/1/11)
- Kassin, S. A., Weiner, B. J., Faber, S. M., et al. 2012, *ApJ*, 758, 106, doi: [10.1088/0004-637X/758/2/106](https://doi.org/10.1088/0004-637X/758/2/106)
- Kingma, D. P., & Ba, J. 2014, ArXiv e-prints. <https://arxiv.org/abs/1412.6980>
- Kretschmer, M., Dekel, A., & Teyssier, R. 2022, *MNRAS*, 510, 3266, doi: [10.1093/mnras/stab3648](https://doi.org/10.1093/mnras/stab3648)
- Law, D. R., Steidel, C. C., Erb, D. K., et al. 2007, *ApJ*, 669, 929, doi: [10.1086/521786](https://doi.org/10.1086/521786)
- Law, D. R., Steidel, C. C., Shapley, A. E., et al. 2012, *ApJ*, 745, 85, doi: [10.1088/0004-637X/745/1/85](https://doi.org/10.1088/0004-637X/745/1/85)
- Lelli, F., Di Teodoro, E. M., Fraternali, F., et al. 2021, *Science*, 371, 713, doi: [10.1126/science.abc1893](https://doi.org/10.1126/science.abc1893)
- Libeskind, N. I., Carlesi, E., Grand, R. J. J., et al. 2020, *MNRAS*, 498, 2968, doi: [10.1093/mnras/staa2541](https://doi.org/10.1093/mnras/staa2541)
- Marinacci, F., Pakmor, R., & Springel, V. 2014, *MNRAS*, 437, 1750, doi: [10.1093/mnras/stt2003](https://doi.org/10.1093/mnras/stt2003)
- Neeleman, M., Prochaska, J. X., Kanekar, N., & Rafelski, M. 2020, *Nature*, 581, 269, doi: [10.1038/s41586-020-2276-y](https://doi.org/10.1038/s41586-020-2276-y)
- Nelson, E. J., Suess, K. A., Bezanson, R., et al. 2022, arXiv e-prints, arXiv:2208.01630. <https://arxiv.org/abs/2208.01630>
- Perrin, M. D., Sivaramakrishnan, A., Lajoie, C.-P., et al. 2014, in *Society of Photo-Optical Instrumentation Engineers (SPIE) Conference Series*, Vol. 9143, *Space Telescopes and Instrumentation 2014: Optical, Infrared, and Millimeter Wave*, ed. J. Oschmann, Jacobus M., M. Clampin, G. G. Fazio, & H. A. MacEwen, 91433X, doi: [10.1117/12.2056689](https://doi.org/10.1117/12.2056689)
- Pillepich, A., Nelson, D., Springel, V., et al. 2019, *MNRAS*, 490, 3196, doi: [10.1093/mnras/stz2338](https://doi.org/10.1093/mnras/stz2338)
- Planck Collaboration, Aghanim, N., Akrami, Y., et al. 2020, *A&A*, 641, A6, doi: [10.1051/0004-6361/201833910](https://doi.org/10.1051/0004-6361/201833910)
- Price, S. H., Kriek, M., Barro, G., et al. 2020, *ApJ*, 894, 91, doi: [10.3847/1538-4357/ab7990](https://doi.org/10.3847/1538-4357/ab7990)
- Rigby, J., Perrin, M., McElwain, M., et al. 2022, arXiv e-prints, arXiv:2207.05632. <https://arxiv.org/abs/2207.05632>
- Rizzo, F., Vegetti, S., Fraternali, F., Stacey, H. R., & Powell, D. 2021, *MNRAS*, 507, 3952, doi: [10.1093/mnras/stab2295](https://doi.org/10.1093/mnras/stab2295)

- Rizzo, F., Vegetti, S., Powell, D., et al. 2020, *Nature*, 584, 201, doi: [10.1038/s41586-020-2572-6](https://doi.org/10.1038/s41586-020-2572-6)
- Robertson, B., Bullock, J. S., Cox, T. J., et al. 2006, *ApJ*, 645, 986, doi: [10.1086/504412](https://doi.org/10.1086/504412)
- Robertson, B., Yoshida, N., Springel, V., & Hernquist, L. 2004, *ApJ*, 606, 32, doi: [10.1086/382871](https://doi.org/10.1086/382871)
- Robotham, A. S. G., Taranu, D. S., Tobar, R., Moffett, A., & Driver, S. P. 2017, *MNRAS*, 466, 1513, doi: [10.1093/mnras/stw3039](https://doi.org/10.1093/mnras/stw3039)
- Ronneberger, O., Fischer, P., & Brox, T. 2015, arXiv e-prints, arXiv:1505.04597. <https://arxiv.org/abs/1505.04597>
- Segovia Otero, Á., Renaud, F., & Agertz, O. 2022, arXiv e-prints, arXiv:2206.08379. <https://arxiv.org/abs/2206.08379>
- Sérsic, J. L. 1968, *Atlas de Galaxias Australes*
- Simons, R. C., Kassin, S. A., Weiner, B. J., et al. 2017, *ApJ*, 843, 46, doi: [10.3847/1538-4357/aa740c](https://doi.org/10.3847/1538-4357/aa740c)
- Smit, R., Bouwens, R. J., Carniani, S., et al. 2018, *Nature*, 553, 178, doi: [10.1038/nature24631](https://doi.org/10.1038/nature24631)
- Stefanon, M., Yan, H., Mobasher, B., et al. 2017, *ApJS*, 229, 32, doi: [10.3847/1538-4365/aa66cb](https://doi.org/10.3847/1538-4365/aa66cb)
- Stott, J. P., Swinbank, A. M., Johnson, H. L., et al. 2016, *MNRAS*, 457, 1888, doi: [10.1093/mnras/stw129](https://doi.org/10.1093/mnras/stw129)
- Tiley, A. L., Gillman, S., Cortese, L., et al. 2021, *MNRAS*, 506, 323, doi: [10.1093/mnras/stab1692](https://doi.org/10.1093/mnras/stab1692)
- Tsukui, T., & Iguchi, S. 2021, *Science*, 372, 1201, doi: [10.1126/science.abe9680](https://doi.org/10.1126/science.abe9680)
- Übler, H., Genzel, R., Tacconi, L. J., et al. 2018, *ApJL*, 854, L24, doi: [10.3847/2041-8213/aaacfa](https://doi.org/10.3847/2041-8213/aaacfa)
- van der Wel, A., Chang, Y.-Y., Bell, E. F., et al. 2014, *ApJL*, 792, L6, doi: [10.1088/2041-8205/792/1/L6](https://doi.org/10.1088/2041-8205/792/1/L6)
- Vaswani, A., Shazeer, N., Parmar, N., et al. 2017, arXiv e-prints, arXiv:1706.03762. <https://arxiv.org/abs/1706.03762>
- Wang, X., Girshick, R., Gupta, A., & He, K. 2017, arXiv e-prints, arXiv:1711.07971. <https://arxiv.org/abs/1711.07971>
- Wells, D. C., Greisen, E. W., & Harten, R. H. 1981, *A&AS*, 44, 363
- Wetzel, A. R., Hopkins, P. F., Kim, J.-h., et al. 2016, *ApJL*, 827, L23, doi: [10.3847/2041-8205/827/2/L23](https://doi.org/10.3847/2041-8205/827/2/L23)
- Wisnioski, E., Förster Schreiber, N. M., Fossati, M., et al. 2019, *ApJ*, 886, 124, doi: [10.3847/1538-4357/ab4db8](https://doi.org/10.3847/1538-4357/ab4db8)
- Wu, Y., Cai, Z., Sun, F., et al. 2022, arXiv e-prints, arXiv:2208.08473. <https://arxiv.org/abs/2208.08473>
- Wuyts, S., Förster Schreiber, N. M., Wisnioski, E., et al. 2016, *ApJ*, 831, 149, doi: [10.3847/0004-637X/831/2/149](https://doi.org/10.3847/0004-637X/831/2/149)
- Yue, M., Yang, J., Fan, X., et al. 2021, *ApJ*, 917, 99, doi: [10.3847/1538-4357/ac0af4](https://doi.org/10.3847/1538-4357/ac0af4)
- Zhang, H., Primack, J. R., Faber, S. M., et al. 2019, *MNRAS*, 484, 5170, doi: [10.1093/mnras/stz339](https://doi.org/10.1093/mnras/stz339)